Gas-Phase Ozonolysis of Cycloalkenes: Formation of Highly Oxidized RO2 Radicals and Their Reactions with NO, NO2, SO2, and Other RO2 Radicals

ARTICLE *in* THE JOURNAL OF PHYSICAL CHEMISTRY A · SEPTEMBER 2015

Impact Factor: 2.69 · DOI: 10.1021/acs.jpca.5b07295

8 AUTHORS, INCLUDING:

Torsten Berndt

Leibniz Institute for Tropospheric Research

234 PUBLICATIONS **3,218** CITATIONS

SEE PROFILE

Mikko Sipilä

University of Helsinki

113 PUBLICATIONS **2,368** CITATIONS

SEE PROFILE

Markku Kulmala

University of Helsinki

1,365 PUBLICATIONS **35,735** CITATIONS

SEE PROFILE

Hartmut Herrmann

Leibniz Institute for Tropospheric Research

745 PUBLICATIONS **6,949** CITATIONS

SEE PROFILE

THE JOURNAL OF PHYSICAL CHEMISTRY A

Article

pubs.acs.org/JPCA

Gas-Phase Ozonolysis of Cycloalkenes: Formation of Highly Oxidized RO_2 Radicals and Their Reactions with NO, NO_2, SO_2, and Other RO_2 Radicals

Torsten Berndt,*[,†] Stefanie Richters,[†] Ralf Kaethner,[†] Jens Voigtländer,[†] Frank Stratmann,[†] Mikko Sipilä,[‡] Markku Kulmala,[‡] and Hartmut Herrmann[†]

[†]Leibniz Institute for Tropospheric Research, TROPOS, 04318 Leipzig, Germany

[‡]Department of Physics, University of Helsinki, P.O. Box 64, Helsinki 00014, Finland

Supporting Information

ABSTRACT: The gas-phase reaction of ozone with C_5−C_8 cycloalkenes has been investigated in a free-jet flow system at atmospheric pressure and a temperature of 297 ± 1 K. Highly oxidized RO_2 radicals bearing at least 5 O atoms in the molecule and their subsequent reaction products were detected in most cases by means of nitrate-CI-APi-TOF mass spectrometry. Starting from a Criegee intermediate after splitting-off an OH-radical, the formation of these RO_2 radicals can be explained via an autoxidation mechanism, meaning RO_2 isomerization (ROO → QOOH) and subsequently O_2 addition (QOOH + O_2 → R′OO). Time-dependent RO_2 radical measurements concerning the ozonolysis of cyclohexene indicate rate coefficients of the intramolecular H-shifts, ROO → QOOH, higher than 1 s^{-1}. The total molar yield of highly oxidized products (predominantly RO_2 radicals) from C_5−C_8 cycloalkenes in air is 4.8−6.0% affected with a calibration uncertainty by a factor of about two. For the most abundant RO_2 radical from cyclohexene ozonolysis, O,O−$C_6H_7(OOH)_2O_2$ ("O,O" stands for two O atoms arising from the ozone attack), the determination of the rate coefficients of the reaction with NO_2, NO, and SO_2 yielded (1.6 ± 0.5) × 10^{-12}, (3.4 ± 0.9) × 10^{-11}, and <10^{-14} cm^3 $molecule^{-1}$ s^{-1}, respectively. The reaction of highly oxidized RO_2 radicals with other peroxy radicals ($R'O_2$) leads to detectable accretion products, RO_2 + $R'O_2$ → ROOR′ + O_2, which allows to acquire information on peroxy radicals not directly measurable with the nitrate ionization technique applied here. Additional experiments using acetate as the charger ion confirm conclusively the existence of highly oxidized RO_2 radicals and closed-shell products. Other reaction products, detectable with this ionization technique, give a deeper insight in the reaction mechanism of cyclohexene ozonolysis.

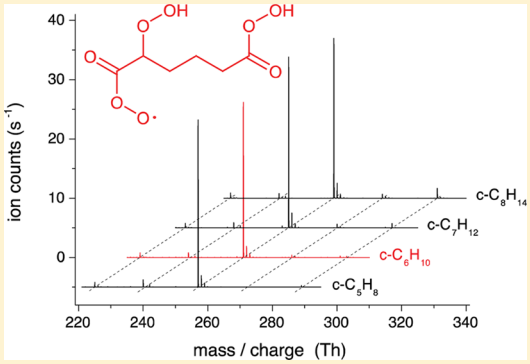

1. INTRODUCTION

Research in the field of hydrocarbon oxidation processes still plays a central role in atmospheric chemistry despite the large effort in the last decades.[1] Degradation mechanisms of biogenic hydrocarbons with the highest emission rates (isoprene, terpenes)[2] as well as their impact for the oxidant budget[3] and the importance of their oxidation products for particle growth[4] are not well understood. Progress in the understanding of these processes is often connected to improvements of analytical techniques.

By this means, an important step in understanding of the role of biogenic oxidation products for the process of SOA (secondary organic aerosol) formation has been achieved applying latest developments of mass spectrometric techniques originally designed for atmospheric OH-radical and H_2SO_4 measurements.[5,6] Ehn et al. recently observed the formation of highly oxidized multifunctional organic compounds (HOMs) from gas-phase oxidation of α-pinene in a smog chamber, as well as from atmospheric measurements in a boreal forest.[7,8] HOMs are believed to comprise hydroperoxy and carbonyl groups, and their vapor pressure is expected to be very low allowing to ascribe HOMs to the class of extremely low-volatility organic compounds (ELVOCs).[9] HOM formation can be explained with the help of a RO_2 radical mechanism[8,10] similar to the autoxidation in the liquid phase that is already known since more than 100 years.[11,12] Experiments on the gas-phase ozonolysis of the most abundant monoterpenes, limonene and α-pinene, demonstrated that highly oxidized RO_2 radicals with up to 12 O atoms, and the corresponding closed-shell products are formed on a time scale of seconds.[10]

A step-by-step O_2 insertion in these RO_2 radicals proceeds very likely via repetitive intramolecular H-shift forming a hydroperoxide moiety, ROO → QOOH, and subsequent O_2 addition forming a next $R'O_2$ radical, QOOH + O_2 → R′OO.[8,10,13] Such intramolecular H-shifts of RO_2 radicals are important pathways for chain propagation in combustion

Received: July 28, 2015
Revised: September 21, 2015
Published: September 22, 2015

DOI: 10.1021/acs.jpca.5b07295
J. Phys. Chem. A 2015, 119, 10336−10348

processes.[14,15] But even for as low as atmospheric temperature this reaction path can be effective for RO_2 chemistry in competition with bimolecular reactions with trace gases. Recently, Crounse et al.[16,17] observed rate coefficients of up to 0.5 s^{-1} at room temperature for intramolecular H-shifts based on product studies from the OH-radical initiated oxidation of methacrolein and 3-pentanone and supported the data by quantum-chemical calculation. Rissanen et al.[13] reported rate coefficients for the intramolecular H-shift of RO_2 radicals from cyclohexene ozonolysis clearly higher than 1 s^{-1} as a result of quantum-chemical calculations.

Formation of the closed-shell HOM products is expected to occur either via unimolecular steps of the highly oxidized RO_2 radicals including OH-radical release or via bimolecular reactions with HO_2, NO, NO_2, or other RO_2 radicals.[8,10,13,18] Two recent studies focused on the formation of these closed-shell products starting from the ozonolysis of cyclohexene or other cycloalkenes.[13,18] Especially cyclohexene serves as model substance with an endocyclic double bond which represents the reactive structural element of the important terpenes, such as α-pinene, limonene, and 3-carene.

In this study, special attention is drawn to the formation pathway and atmospheric reactions of highly oxidized RO_2 radicals from ozonolysis of C_5−C_8 cycloalkenes. Up to now, highly oxidized RO_2 radicals and subsequent closed-shell products were almost exclusively detected as NO_3^- adducts. A comparison of results from different ionization techniques, i.e., using nitrate or acetate ionization, allows to assess the reliability of findings from the nitrate ionization technique. Results of the present study should contribute to a better understanding of the reaction mechanism of gas-phase ozonolysis of cycloalkenes such as the most important terpenes with a cycloalkene structure.

2. EXPERIMENTAL SECTION

2.1. Free-Jet Flow System. The gas-phase reaction of ozone with C_5−C_8 cycloalkenes has been conducted in a free-jet flow system (outer tube: length: 200 cm, 15 cm i.d. and a moveable inner tube: 9.5 mm o.d. with a 3 mm i.d. nozzle) at T = 297 ± 1 K and 1 bar pressure of purified air or variable N_2/O_2 mixtures; see schematic in Figure 1. This experimental approach allows investigations under nearly wall-free conditions and with reaction times of 1.5−7.9 s.[19]

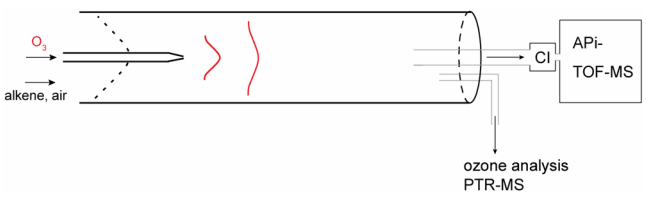

Figure 1. Schematic of the experimental set up of the free-jet flow system including the sampling for gas-phase analysis. The red wavy lines illustrate the development of the ozone/cycloalkene plume.

The inner flow (5 L min^{-1} STP) containing ozone diluted in air or a N_2/O_2 mixture is injected through a nozzle into the main gas stream (95 L min^{-1} STP) comprising the second reactant (cycloalkene) mixed in the carrier gas. Rapid mixing of the two gas streams takes place downstream the nozzle exit ensuring homogeneously mixed reactant conditions.[20] Development of the ozone/cycloalkene plume is demonstrated schematically by the red wavy lines in Figure 1. For the center flow, diffusion-controlled losses of species can be neglected for the time range of this experiment. Numerical simulations by means of computational fluid dynamics (CFD) have been performed in order to characterize the flow conditions and the reactant mixing in the system.[19] The reaction time for a given distance between nozzle and sampling point of the mass spectrometer was experimentally determined using the reaction of ozone with TME (2,3-dimethyl-2-butene) as a "chemical clock". Experimentally obtained reaction times in this way were in a good agreement with the findings from CFD modeling.[19]

Ozone was produced by passing air through an ozone generator (UVP OG-2). All gas flows were set by calibrated gas flow controllers (MKS 1259/1179). The reactant gases used had the following purities: c-C_5H_8 (Aldrich, 96%), c-C_6H_{10} (Fluka, ≥ 99.5%), c-C_7H_{12} (Aldrich, 97%), c-C_8H_{14} (Aldrich, ≥ 99.5%), CH_3COOH (Aldrich, 99.5%), $^{13}CH_3COOH$ (Aldrich, 99 atom % ^{13}C), and $C_6H_3(CH_3)_3$ (mesitylene, 1,3,5-trimethylbenzene) (Fluka, 99%). Air was taken from a PSA (pressure swing adsorption) unit with further purification by activated charcoal, 4 Å molecular sieve, and subsequently by GateKeeper CE-2500KH084R (Entegris) for the removal of trace impurities by means of inorganic media. The water vapor concentration of the purified (dry) air was $<10^{13}$ molecules cm^{-3} as checked by means of FT-IR measurements.[19] Different oxygen contents in the carrier gas were achieved by mixing nitrogen (AirProducts, 99.9997%) with air in different amounts. If needed, humidified air was produced by passing a part of the pressure gas through water saturators filled either with H_2O (ultrapure water system Barnstead, resistivity: 17.4 MΩ cm) or D_2O (Aldrich, 99.9 atom %).

Ozone concentrations were measured at the outflow of the reactor by a gas monitor (Thermo Environmental Instruments 49C). A proton transfer reaction - mass spectrometer (PTR-MS; HS PTR-QMS 500, Ionicon)[21] served as an online monitor for the cycloalkenes.

The amount of reacted cycloalkene by ozonolysis was calculated according to $\text{reacted[cycloalkene]} = k_{\text{cycloalkene}+O_3}[O_3][\text{cycloalkene}]\ t$. Low reactant conversion smaller than 1% justified this approach. The needed rate coefficients were taken from literature (unit: cm^3 $molecule^{-1}$ s^{-1}): $k_{\text{cyclopentene}+O_3}$ = 6.54 × 10^{-16},[22] $k_{\text{cyclohexene}+O_3}$ = 7.46 × 10^{-17},[22] $k_{\text{cycloheptene}+O_3}$ = 2.49 × 10^{-16},[23] and $k_{\text{cyclooctene}+O_3}$ = 3.77 × 10^{-16}.[23]

2.2. Product Detection and Determination of Concentrations. The detection of HOMs was carried out in the most cases (see below) by means of nitrate-CI-APi-TOF (chemical ionization−atmospheric pressure interface−time-of-flight) mass spectrometry (Airmodus, Tofwerk) sampling from the center flow with a rate of 10 L min^{-1} (STP).[5−7,24,25] A flow of 1−2 mL min^{-1} air over a concentrated nitric acid (HNO_3) sample was added to a 35 L min^{-1} (STP) flow of purified air producing the HNO_3 containing sheath air that forms the charger ions, NO_3^-, $(HNO_3)NO_3^-$, and $(HNO_3)_2NO_3^-$, after ionization with a ^{241}Am source. The ions from the sheath flow are electrostatically sucked into the sample flow (in the middle of the CI-inlet) without mixing of both streams. Highly oxidized multifunctional organic compounds (HOMs) are able to form stable $(HOM)NO_3^-$ adducts allowing their detection with high sensitivity.[8,26] A recent, theoretical work indicates that at least two hydrogen bond donor functional groups must be present in the HOM to form a stable $(HOM)NO_3^-$ adduct.[26] The detection sensitivity of these $(HOM)NO_3^-$

DOI: 10.1021/acs.jpca.5b07295
J. Phys. Chem. A 2015, 119, 10336−10348

adducts is assumed to be nearly constant for molecules with at least two OH- or OOH-groups in addition to two carbonyl groups.[18] HOM concentrations (radicals and closed-shell products) were determined according to eq I:

$$[\mathrm{HOM}] = f_{\mathrm{HOM,nitrate}} \times \frac{[(\mathrm{HOM})\mathrm{NO_3^-}]}{[\mathrm{NO_3^-}] + [(\mathrm{HNO_3})\mathrm{NO_3^-}] + [(\mathrm{HNO_3})_2\mathrm{NO_3^-}]} \quad (\mathrm{I})$$

The quantities in eq I, $[(\mathrm{HOM})\mathrm{NO_3^-}]$, etc., are the measured signal intensities. An absolute signal calibration with reference substances, however, is impossible due to the lack of an independent way of defined HOM synthesis. Therefore, the absolute H_2SO_4 calibration factor experimentally determined for this detection system was used in order to calculate HOM concentrations, $f_{\mathrm{HOM,nitrate}} = f_{\mathrm{H2SO4,exp}}$.[27] This approach assumes that $(\mathrm{HOM})\mathrm{NO_3^-}$ adduct formation in the CI-inlet via reaction 1

$$\mathrm{HOM} + (\mathrm{HNO_3})_n\mathrm{NO_3^-} \rightarrow (\mathrm{HOM})\mathrm{NO_3^-} + (\mathrm{HNO_3})_n \quad n = 0, 1, 2 \quad (1)$$

proceeds with the same efficiency as the generation of $\mathrm{HSO_4^-}$ and $(\mathrm{HNO_3})\mathrm{HSO_4^-}$ from the corresponding reaction of H_2SO_4, reactions 2a and 2b.[8]

$$\mathrm{H_2SO_4} + (\mathrm{HNO_3})_n\mathrm{NO_3^-} \rightarrow \mathrm{HSO_4^-} + (\mathrm{HNO_3})_{n+1} \quad (2a)$$

$$\rightarrow (\mathrm{HNO_3})(\mathrm{HSO_4^-}) + (\mathrm{HNO_3})_n \quad n = 0, 1, 2 \quad (2b)$$

It is to be noted that the experimental H_2SO_4 calibration factor $f_{\mathrm{H2SO4,exp}} = 1.85 \times 10^9$ molecules $\mathrm{cm^{-3}}$ lies within the range of the calculated factor[28] $f_{\mathrm{H2SO4,calc}} = (1.5–2.8) \times 10^9$ molecules $\mathrm{cm^{-3}}$ taking into account a 12% diffusion loss of the reactant (H_2SO_4) in the short inlet tube, a reaction time of the ion–molecule reaction of 0.2–0.3 s, and corresponding rate coefficients $k_{2a} + k_{2b} = (2–2.5) \times 10^{-9}$ $\mathrm{cm^3}$ $\mathrm{molecule^{-1}}$ $\mathrm{s^{-1}}$.[29] The good agreement of $f_{\mathrm{H2SO4,exp}}$ with $f_{\mathrm{H2SO4,calc}}$ indicates that this simple calculation describes ionization and subsequent ion detection properly. The rate coefficient k_1 is expected to be similar to $k_{2a} + k_{2b}$, typical for ion–molecule reactions close to the collision limit.[28,29] With this assumption for k_1, the calculated value of $f_{\mathrm{HOM,nitrate}}$ is equal to $f_{\mathrm{H2SO4,calc}}$ assuming again a 12% diffusion loss of HOMs in the short inlet tube. Therefore, $f_{\mathrm{H2SO4,exp}}$ could be used as a good approximation for the lower-end value of the HOM calibration factor. Thus, resulting HOM concentrations can be treated as lower limit values affected by an approximated uncertainty factor of 2 due to the error of the calibration factor itself and possible differences in the ion transmission efficiencies of $(\mathrm{HOM})\mathrm{NO_3^-}$ and $\mathrm{HSO_4^-}$ /$(\mathrm{HNO_3})\mathrm{HSO_4^-}$. The detection limit is about 10^4 molecules $\mathrm{cm^{-3}}$ when applying 2 min data averaging.

In a few experiments, atmospheric pressure CI was carried out using $(\mathrm{CH_3COOH})_m\mathrm{CH_3COO^-}$ (m = 0, 1, 2) as charger ions instead of $(\mathrm{HNO_3})_n\mathrm{NO_3^-}$.[30–32] In this case, a flow of 5 mL $\mathrm{min^{-1}}$ of purified air over an acetic acid sample was added to the sheath air. The ion–molecule reaction proceeds either via proton transfer from the target molecule to the charger ion, reaction 3a, or via adduct formation, reaction 3b.[33]

$$\mathrm{HOM} + (\mathrm{CH_3COOH})_m\mathrm{CH_3COO^-} \rightarrow (\mathrm{HOM{-}H})^- + (\mathrm{CH_3COOH})_{m+1} \quad (3a)$$

$$\rightarrow (\mathrm{HOM})\mathrm{CH_3COO^-} + (\mathrm{CH_3COOH})_m \quad m = 0, 1, 2 \quad (3b)$$

Here, $(\mathrm{HOM{-}H})^-$ stands for the deprotonation product of a HOM (the conjugated base). HOM concentrations from runs with $(\mathrm{CH_3COOH})_m\mathrm{CH_3COO^-}$ as charger ions were calculated according to eq II:

$$[\mathrm{HOM}] = f_{\mathrm{HOM,acetate}} \times \frac{[(\mathrm{HOM{-}H})^-] + [(\mathrm{HOM})\mathrm{CH_3COO^-}]}{[\mathrm{CH_3COO^-}] + [(\mathrm{CH_3COOH})\mathrm{CH_3COO^-}] + [(\mathrm{CH_3COOH})_2\mathrm{CH_3COO^-}]} \quad (\mathrm{II})$$

The calibration factor $f_{\mathrm{HOM,acetate}}$ was set equal to $f_{\mathrm{HOM,nitrate}}$ assuming again a similar reactivity of acetate(cluster) ions and nitrate(cluster) ions toward HOMs, i.e., $(k_{2a} + k_{2b}) \sim (k_{3a} + k_{3b}) \sim k_1$. Unambiguous attribution of detected signals either to a deprotonated species from reaction 3a or to an adduct from reaction 3b was possible applying labeled acetic acid ($^{13}\mathrm{CH_3COOH}$) instead of the unlabeled species for charger ion formation.

Charger ion spectra of $(\mathrm{HNO_3})_n\mathrm{NO_3^-}$, $(\mathrm{CH_3COOH})_m\mathrm{CH_3COO^-}$, and $(^{13}\mathrm{CH_3COOH})_m{}^{13}\mathrm{CH_3COO^-}$ are shown in Figures S1a–c in the Supporting Information. Identical voltage settings were applied for both ionization techniques as optimized for low fragmentation measurements in the nitrate ionization mode.

3. RESULTS AND DISCUSSION

3.1. NO_3^--Adduct Spectra and HOM Concentrations.

Figure 2 shows the spectrum range of the most important signals observed from ozonolysis of C_5–C_8 cycloalkenes for reacted cycloalkene of (4.6–5.4) × 10^8 molecules $\mathrm{cm^{-3}}$. Experiments in the presence of OH-radical scavengers (propane, cyclohexane, or mesitylene) showed no differences in this range indicating that all signals arose from ozonolysis products.

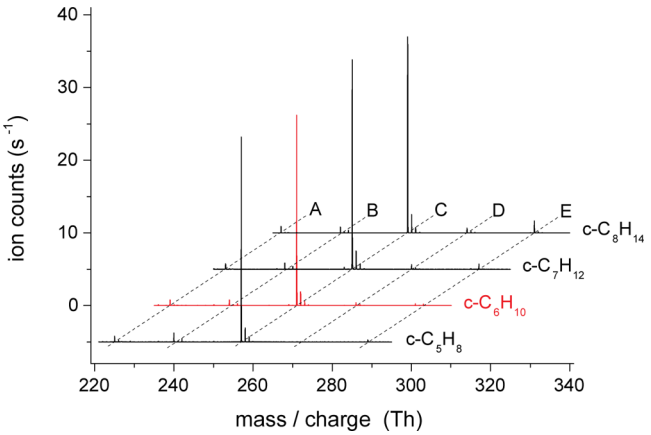

Figure 2. Spectra of $(\mathrm{HOM})\mathrm{NO_3^-}$ adducts from the ozonolysis of C_5–C_8 cycloalkenes in the mass/charge range of 220–340 Th. Signals A, C, and E are attributed to highly oxidized RO_2 radicals, O,O–$C_nH_{2n-3-x}(OOH)_xO_2$ with n = 5–8 (number of the carbon atoms) and x = 1–3 (number of OOH groups; A: x = 1, C: x = 2 and E: x = 3). The signals B and D are assigned to closed-shell products O,O–$C_nH_{2n-4-x}O(OOH)_x$ with x = 2 or 3 (B: x = 2 and D: x = 3). $[O_3]$ = 6.1×10^{11}, [c-C_5H_8] = 1.7×10^{11}, [c-C_6H_{10}] = 1.26×10^{12}, [c-C_7H_{12}] = 4.14×10^{11}, and [c-C_8H_{14}] = 2.84×10^{11} molecules $\mathrm{cm^{-3}}$, reaction time: 7.9 s.

DOI: 10.1021/acs.jpca.5b07295
J. Phys. Chem. A 2015, 119, 10336–10348

All four spectra show the same features shifted by 14 mass units (CH_2−group) switching from one cycloalkene to the next, e.g., from cyclopentene to cyclohexene etc. The signals A, C, and E can be attributed to RO_2 radicals characterized by the general formula $O,O{-}C_nH_{2n-3-x}(OOH)_xO_2$ with n = 5−8 (number of the carbon atoms) and x = 1−3 (number of OOH groups in the molecule; A: x = 1, C: x = 2, and E: x = 3). "O,O" in this formula stands for two O atoms arising from the attacking ozone. The same notation has already been used for the description of highly oxidized RO_2 radicals from ozonolysis of limonene and α-pinene.[10] The number of acidic H atoms in the molecule (here equal to the number of OOH groups x) was confirmed in experiments with D_2O additions in the pressure gas measuring the signal shift in the mass spectrum caused by H/D exchange.[13] In Figure S2, a comparison of the mass spectra recorded in absence and presence of D_2O is given for an experiment of the ozonolysis of cyclohexene. The assignment of the signals A, C, and E to RO_2 radicals appears to be justified because of the detected reaction products from the reaction with NO_x or with other RO_2 radicals, i.e., formation of organic nitrates from the reaction with NO, peroxynitrates from the reaction with NO_2, and accretion products ROOR′ from the reaction with other $R'O_2$ radicals, see later. The RO_2 radical with two OOH-groups ($O,O{-}C_nH_{2n-5}(OOH)_2O_2$, n = 5−8) represents the predominant signal in the spectrum in each case, signal C in Figure 2. Former studies on the ozonolysis of C_5 − C_7 cycloalkenes using a similar detection technique reported no RO_2 radicals[13] or smaller RO_2 radical signals[18] besides signals of different closed-shell products. In the latter study,[18] the RO_2 radical with two OOH-groups was also the most abundant RO_2 radical in line with our finding. Differences in the observed product spectra can be partly explained by lower reactant concentrations and a shorter reaction time in our experiments reducing consecutive reactions of formed RO_2 radicals. The small signals B and D can be explained by the occurrence of closed-shell products $O,O{-}C_nH_{2n-4-x}O(OOH)_x$ with x = 2 or 3 (B: x = 2 and D: x = 3) formed after formal loss of OH from the corresponding RO_2 radical.[8,10,13,18]

Additionally, further signals with relatively low intensity have been observed attributed to a next class of RO_2 radicals. Their composition points to a CO splitting-off in the course of their generation leading to the general formula $O{-}C_{n-1}H_{2n-3-\alpha}(OOH)_\alpha O_2$ (n: number of the carbon atoms; and α: number of OOH groups). Results from theoretical calculations by Rissanen et al.[13] indicated a negligible importance of CO splitting-off for the product distribution from the ozonolysis of cyclohexene.

RO_2 radical concentrations ($O,O{-}C_6H_{9-x}(OOH)_xO_2$ for x = 1−3 and $O{-}C_5H_{9-\alpha}(OOH)_\alpha O_2$ formed after CO splitting-off for α = 1,2) and concentrations of closed-shell products ($C_6H_8O_7$ and $C_6H_8O_9$, signals B and D in Figure 2) from cyclohexene ozonolysis are depicted in Figure 3 as a function of converted cyclohexene. The concentrations were calculated according to eq I representing lower limit values. For RO_2 radicals with a single OOH group (x = 1: $O,O{-}C_6H_8(OOH)O_2$ and α = 1: $O{-}C_5H_8(OOH)O_2$) the given concentrations represent most likely a distinct underestimation (relative to the other RO_2) due to the expected lower stability of these $(HOM)NO_3^-$ adducts.[18,26] The RO_2 concentrations increase proportionally with increasing cyclohexene; i.e., the slope $[RO_2]$ vs reacted cyclohexene is very close to 1. RO_2 radical conversion becomes only significant for the highest cyclohexene conversion of a few 10^9 molecules cm^{-3} indicated by a slight curvature of the RO_2 concentrations with rising cyclohexene conversion. The concentrations of the closed-shell products $C_6H_8O_7$ and $C_6H_8O_9$ ($O,O{-}C_6H_{8-x}O(OOH)_x$ with x = 2 or 3) show a slope of about two with respect to reacted cyclohexene. This behavior indicates that these products are formed in bimolecular steps, very likely from the reaction of the highly oxidized RO_2 radicals with other RO_2 radicals in the system.[8,10,13,18] Corresponding RO_2 radicals and closed-shell products with a similar behavior have been detected in the case of the ozonolysis of cyclopentene, cycloheptene and cyclooctene as well, see Figures S4a, S5a, and S6a, respectively.

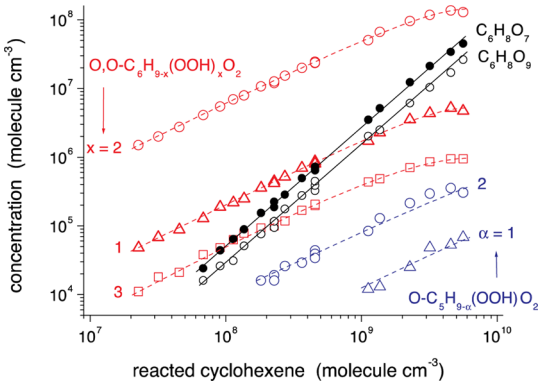

Figure 3. Concentrations of highly oxidized RO_2 radicals ($O,O{-}C_6H_{9-x}(OOH)_xO_2$ with x = 1−3, red, and $O{-}C_5H_{9-\alpha}(OOH)_\alpha O_2$ with α = 1,2, blue) and the most abundant closed-shell products $C_6H_8O_7$ and $C_6H_8O_9$ ($O,O{-}C_6H_{8-x}O(OOH)_x$ with x = 2 or 3, black) as a function of reacted cyclohexene (nitrate ionization). $[O_3] = 6.1 \times 10^{11}$ and $[c\text{-}C_6H_{10}] = (6.3{-}1560) \times 10^{10}$ molecules cm^{-3}, reaction time: 7.9 s.

3.2. Formation of Accretion Products. In Figure 4, a mass spectrum from cyclohexene ozonolysis in the range 335−455 Th is shown, comprising the signals of accretion products explained by ROOR′, $(ROOR')NO_3^-$ adducts, from the reaction $RO_2 + R'O_2$. Concentrations of the most abundant accretion products as a function of reacted cyclohexene are depicted in Figure S3. The accretion product concentrations

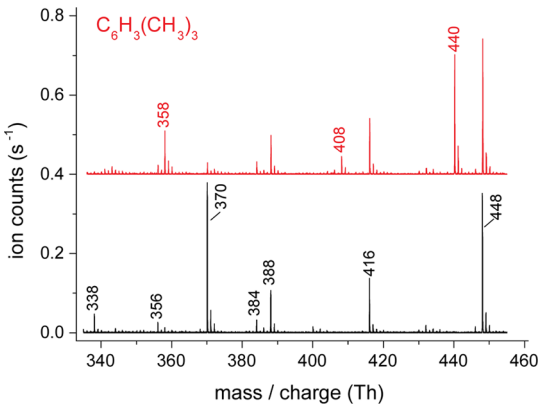

Figure 4. Mass spectra from the ozonolysis of $c\text{-}C_6H_{10}$ detected in the range of the accretion products, 335−455 Th, in absence (lower part, black) or presence (upper part, red) of mesitylene (1,3,5-trimethylbenzene) acting as OH radical scavenger (nitrate ionization). Given numbers are the nominal mass/charge values of the NO_3^- adducts. $[O_3] = 6.1 \times 10^{11}$, $[c\text{-}C_6H_{10}] = 3.0 \times 10^{12}$, and $[C_6H_3(CH_3)_3] = 5.2 \times 10^{13}$ molecules cm^{-3}, reaction time: 7.9 s.

DOI: 10.1021/acs.jpca.5b07295
J. Phys. Chem. A 2015, 119, 10336−10348

Table 1. Accretion Products ROOR′ from the Reaction of RO_2 + $R'O_2$ → ROOR′ + O_2, Ozonolysis of c-C_6H_{10}, cf. Figure 4[a]

	O,O-$C_6H_7(OOH)_2O_2$ $C_6H_9O_8$	O,O-$C_6H_8(OOH)O_2$ $C_6H_9O_6$
O,O-$C_6H_7(OOH)_2O_2$ $C_6H_9O_8$	$C_{12}H_{18}O_{14}$ strong (448, 4)	…
O,O-$C_6H_8(OOH)O_2$ $C_6H_9O_6$	$C_{12}H_{18}O_{12}$ medium (416, 3)	…
O,O-$C_6H_9O_2$ $C_6H_9O_4$	$C_{12}H_{18}O_{10}$ weak (384, 2)	$C_{12}H_{18}O_8$ not detected (352)
O-$C_5H_8(OOH)O_2$ $C_5H_9O_5$ (from CO splitting-off)	$C_{11}H_{18}O_{11}$ medium (388, 3)	$C_{11}H_{18}O_9$ weak (356, 2)
HO-$C_6H_{10}O_2$ $C_6H_{11}O_3$ (from OH + c-C_6H_{10})	$C_{12}H_{20}O_9$ strong (370, 3)	$C_{12}H_{20}O_7$ weak (338, 2)
HO-$C_6H_3(CH_3)_3(OO)O_2$ $C_9H_{13}O_5$ (from OH + mesitylene)	$C_{15}H_{22}O_{11}$ strong (440, 3)	$C_{15}H_{22}O_9$ weak (408, 2)

[a]Given numbers in brackets (XYZ, B) are the observed nominal mass/charge values of the NO_3^- adduct (XYZ) and the number of acidic H-atoms (B) measured in the presence of D_2O according to the signal shift from H/D exchange. The arrows indicate symmetric reactions. Information concerning the signal intensity (strong, medium, weak, or not detected) is provided as well.

depending on reacted cycloalkene from the ozonolysis of cyclopentene, cycloheptene and cyclooctene are given in Figures S4b, S5b, and S6b, respectively. In the lower part of the spectrum in Figure 4, which was recorded in absence of an OH-radical scavenger, the nominal mass/charge values at 384, 416, and 448 Th are attributed to $(ROOR')NO_3^-$ adducts where RO_2 and $R'O_2$ are O,O−$C_6H_{9-x}(OOH)_xO_2$ with x = 0−2. Signals at 356 and 388 Th are attributed to products from the reaction of O,O−$C_6H_{9-x}(OOH)_xO_2$ (x = 1,2) with O−$C_5H_{9-\alpha}(OOH)_\alpha O_2$ (α = 1,2) and those at 338 and 370 Th from the reaction of O,O−$C_6H_{9-x}(OOH)_xO_2$ (x = 1,2) with HO-$C_6H_{10}O_2$. HO-$C_6H_{10}O_2$ is formed from the reaction of OH-radicals with cyclohexene and subsequent O_2 addition. OH-radical generation from the ozonolysis of cyclohexene is reported with a yield of 68%.[34] Experiments in the presence of OH-radical scavengers were conducted in order to confirm the signal assignment.

The upper part of the spectrum in Figure 4 shows the results in the presence of mesitylene (1,3,5-trimethylbenzene, $C_6H_3(CH_3)_3$). With exception of the signals at 338 and 370 Th (attributed to products of HO-$C_6H_{10}O_2$), all other signals from the run without mesitylene remained unchanged. New appearing signals at 408 and 440 Th are likely due to products from the reaction of O,O−$C_6H_{9-x}(OOH)_xO_2$ (x = 1,2) with HO-$C_6H_3(CH_3)_3(OO)O_2$. The latter is the internal O_2-bridged RO_2 radical from the addition of OH radicals on mesitylene.[35,36] For the additional signal at 358 Th, there is no justifiable attribution at the moment. In the following the structures of HO-$C_6H_{10}O_2$ and HO-$C_6H_3(CH_3)_3(OO)O_2$ are depicted:

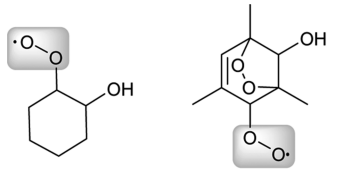

HO-$C_6H_{10}O_2$ HO-$C_6H_3(CH_3)_3(OO)O_2$

Table 1 summarizes the identified accretion products observed in absence and presence of mesitylene. The number of OOH groups in these compounds, according to the expected composition, was validated in experiments with D_2O addition measuring again the signal shift in the mass spectrum due to the H/D exchange in the OOH groups.

This analysis shows that also other RO_2 radicals, not directly observable as NO_3^- adduct, can be indirectly identified via their accretion products from the reaction with highly oxidized RO_2 radicals, at least qualitatively.

3.3. Comparison: Acetate vs Nitrate Ionization (Ozonolysis of Cyclohexene). A comparison of results using either CH_3COO^-(clusters) or NO_3^-(clusters) in the ionization process has been conducted to assess the reliability of findings from the nitrate ionization technique. This latter technique was used so far almost exclusively for direct detection of HOMs.[8,10,13,18,37] "Normal" CH_3COO^- and $^{13}CH_3COO^-$ was applied alternately in order to distinguish between deprotonation products and adducts formed by acetate ionization via reactions 3a and 3b, respectively. Figure 5 shows a mass spectrum from the ozonolysis of cyclohexene recorded in the range of the strongest signals (200−280 Th) using labeled and nonlabeled acetate(cluster) ions. A shift of a certain signal by one mass unit indicates the presence of an

DOI: 10.1021/acs.jpca.5b07295
J. Phys. Chem. A 2015, 119, 10336−10348

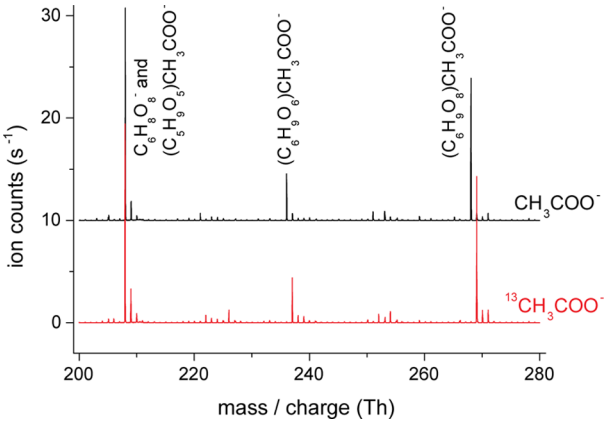

Figure 5. Mass spectra in the range 200−280 Th using either CH_3COO^-(clusters) as charger ions (upper part, black) or $^{13}CH_3COO^-$(clusters) (lower part, red). $(C_6H_9O_6)CH_3COO^-$ is attributed to the cluster adduct of O,O−$C_6H_{9-x}(OOH)_xO_2$ with x = 1, $(C_6H_9O_8)CH_3COO^-$ to the cluster adduct of O,O−$C_6H_{9-x}(OOH)_xO_2$ with x = 2, $C_6H_8O_8^-$ to the deprotonated O,O−$C_6H_{9-x}(OOH)_xO_2$ with x = 2 and $(C_5H_9O_5)CH_3COO^-$ to the cluster adduct of O−$C_5H_{9-\alpha}(OOH)_\alpha O_2$ with α = 1. $[O_3]$ = 6.1 × 10^{11} and [c-C_6H_{10}] = 4.6 × 10^{12} molecules cm^{-3}, reaction time: 7.9 s.

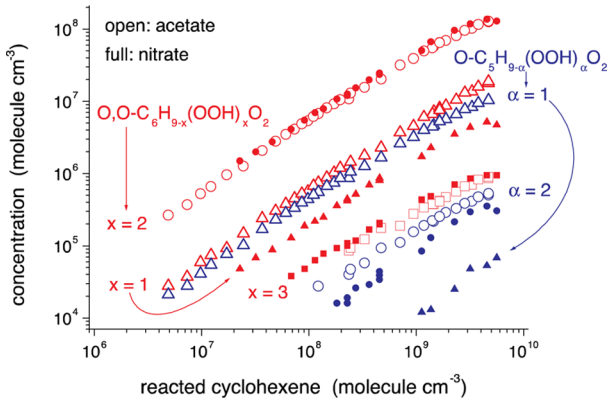

Figure 6. Comparison of highly oxidized RO_2 radical concentrations (O,O−$C_6H_{9-x}(OOH)_xO_2$ with x = 1−3, red, and O−$C_5H_{9-\alpha}(OOH)_\alpha O_2$ with α = 1, 2, blue) determined either by the acetate or nitrate ionization technique for identical reaction conditions. Results depicted for nitrate ionization are identical with those already shown in Figure 3.

adduct utilizing $^{13}CH_3COO^-$ instead of CH_3COO^-. Hence, the signal at the nominal mass/charge ratio of 268 Th can be attributed to the CH_3COO^- adduct of O,O−$C_6H_{9-x}(OOH)_xO_2$ with x = 2, $(C_6H_9O_8)CH_3COO^-$, and that at 236 Th to the adduct of O,O−$C_6H_{9-x}(OOH)_xO_2$ with x = 1, $(C_6H_9O_6)CH_3COO^-$. The exact masses (resolving power of the mass spectrometer: >4000 Th/Th) confirmed the peak composition. For the signal at 208 Th, only a relatively small fraction of the peak shifted to the higher mass using $^{13}CH_3COO^-$ indicating overlapping signals dominated by a deprotonation product. Peak fitting of the signals obtained by CH_3COO^- and $^{13}CH_3COO^-$ ionization revealed that this signal consisted on an average of 88% of the deprotonation product of O,O−$C_6H_{9-x}(OOH)_xO_2$ with x = 2, $C_6H_8O_8$, and 12% of the adduct of O−$C_5H_{9-\alpha}(OOH)_\alpha O_2$ with α = 1, $(C_5H_9O_5)CH_3COO^-$. An example of the result of a peak fitting procedure is given in Figure S7. Analogous treatment of the weak signal at 240 Th (not clearly visible in Figure 5) yielded a composition of 56% of the deprotonation product of O,O−$C_6H_{9-x}(OOH)_xO_2$ with x = 3, $C_6H_8O_{10}$, and 44% of the adduct of O−$C_5H_{9-\alpha}(OOH)_\alpha O_2$ with α = 2, $(C_5H_9O_7)CH_3COO^-$, see Figure S8.

Resulting HOM concentrations (lower limit values) from acetate ionization were calculated according to eq II. Figure 6 shows a comparison of the highly oxidized RO_2 radical concentrations detected from cyclohexene ozonolysis for identical reaction conditions applying acetate (open symbol) or nitrate ionization (full symbol). The agreement of results from both techniques is very good in the case of O,O−$C_6H_{9-x}(OOH)_xO_2$ with x = 2 and 3. Even for the small concentrations of O−$C_5H_{9-\alpha}(OOH)_\alpha O_2$ with α = 2, the agreement is good with a deviation within a factor of 2. On the other hand, there are distinct differences in the case of the RO_2 radicals with a single OOH group. For O,O−$C_6H_{9-x}(OOH)_xO_2$ with x = 1, acetate ionization yielded about three times higher concentrations compared with the results from nitrate ionization. In the case of O−$C_5H_{9-\alpha}(OOH)_\alpha O_2$ with α = 1, the concentrations from acetate ionization were more than 2 orders of magnitude higher than those from nitrate ionization. Thus, it must be concluded that the nitrate technique can considerably underestimate RO_2 concentrations with a single OOH group (relative to the acetate technique) taking into account that the given concentrations represent lower limits each, see section 2.2. Such an underestimation by the nitrate ionization technique is qualitatively in line with the expected stability of $(HOM)NO_3^-$ adducts for HOMs with less than two hydrogen donor groups in the molecule.[26] Up to now there are no theoretical calculations available in the literature describing the stability of $(HOM)CH_3COO^-$ adducts. It could be speculated that the enhanced sensitivity of acetate ionization is partly caused by the fact that the negative charge on acetate is delocalized over only two oxygens, making each O in acetate a stronger hydrogen bond acceptor than each O in nitrate.

The comparison of concentrations from both ionization techniques for the most abundant closed-shell molecules $C_6H_8O_7$ and $C_6H_8O_9$ (O,O−$C_6H_{8-x}O(OOH)_x$ with x = 2 or 3), and for the accretion product $C_{12}H_{20}O_9$ is depicted in Figure S9. The agreement for $C_6H_8O_7$ is good. However, for the other two species, the acetate ionization yields only about one-third of the concentration obtained by the nitrate ionization technique. These data suggest that for closed-shell species the acetate ionization technique can lead to an underestimation of the concentration (relative to the nitrate technique). Here, more comprehensive studies under conditions of enhanced closed-shell HOM formation are needed before a reliable conclusion can be drawn.

Nevertheless, results using the acetate ionization technique show conclusively the existence of highly oxidized RO_2 radicals and closed-shell products in the same way as detected first by nitrate ionization.[7,8]

3.3.1. Other Products Detectable by Acetate Ionization. Chemical ionization by acetate ions allows to detect a relatively broad spectrum of substances, especially carboxylic acids and peroxy carboxylic acids.[30−32] In Figure 7, mass spectra in the range 125−195 Th are depicted observed with labeled and nonlabeled acetate(cluster) ions for the same reactant conditions as used for recording the spectra given in Figure 5. Beside the charger ion signals at the nominal mass/charge ratio of 179 and 182 Th for $(CH_3COOH)_2CH_3COO^-$ and

DOI: 10.1021/acs.jpca.5b07295
J. Phys. Chem. A 2015, 119, 10336−10348

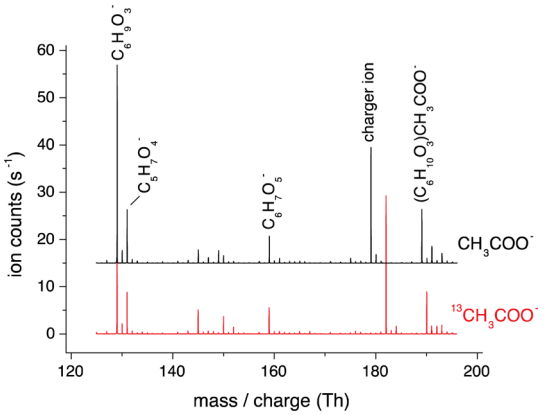

Figure 7. Mass spectra in the range 125−195 Th using as charger ions either CH_3COO^-(clusters) (upper part, black) or $^{13}CH_3COO^-$(clusters) (lower part, red). Signals at the nominal mass/charge ratio of 179 and 182 Th are charger ion signals: $(CH_3COOH)_2CH_3COO^-$ and $(^{13}CH_3COOH)_2{}^{13}CH_3COO^-$. $[O_3]$ = 6.1×10^{11} and $[c\text{-}C_6H_{10}]$ = 4.6×10^{12} molecules cm^{-3}, reaction time: 7.9 s.

$(^{13}CH_3COOH)_2{}^{13}CH_3COO^-$, the strongest signals at 129 and 189 Th (190 Th) were attributed to the deprotonation product and the acetate adduct of a substance with the formula $C_6H_{10}O_3$. The chemical structure of this species is speculative at the moment. Other signals at 131 and 159 Th are consistent with deprotonation products of peroxy carboxylic acids, $C_5H_8O_4$ and $C_6H_8O_5$, representing expected products from unimolecular steps starting from $O,O\text{−}C_6H_{9-x}(OOH)_xO_2$ with x = 1, see formation of species (**9**) and (**11**) in the proposed mechanism, section 3.4. The concentrations of $C_5H_8O_4$ and $C_6H_8O_5$ increase almost proportionally with increasing amount of reacted cyclohexene indicating that both substances are most likely products of unimolecular steps starting from a RO_2 radical; see Figure S10.

3.4. Reaction Mechanism. The reaction mechanism for the ozonolysis of cyclohexene proposed in the following is qualitatively able to explain the formation of all detected RO_2 radicals as well as $C_5H_8O_4$ (**9**) and $C_6H_8O_5$ (**11**), the expected closed-shell products from unimolecular steps after splitting-off an OH-radical. The formation of other species, such as $C_6H_8O_7$ and $C_6H_8O_9$, and accretion products, being products of bimolecular RO_2 reactions, is not considered here. In the following schemes, the solid frames indicate substances detectable by nitrate and acetate ionization, the dashed frames these only detectable using acetate ionization. O atoms arising from attacking ozone are given in blue. This mechanism represents an extension of the RO_2 radical autoxidation scheme given by Rissanen et al.[13]

After the initial attack of ozone toward cyclohexene and subsequent ring cleavage, a Criegee intermediate (**2**) is produced.[38] In an unimolecular step, the Criegee intermediate (**2**) can form a vinyl hydroperoxide that rapidly dissociates producing OH and an alkyl radical.[39,40] The alkyl radical produces the first RO_2 radical (**3**) after O_2 addition.

The RO_2 radical (**3**) can undergo internal H-abstraction in competition with bimolecular steps with other reactants.

Scheme 1. (a) First Steps of the Ozonolysis of Cyclohexene Forming the First RO_2 Radical (In Simplified Terms), (b) Intramolecular H-Abstraction and Subsequent Formation of $O,O\text{−}C_6H_{9-x}(OOH)_xO_2$ with x = 1 (5) and $O\text{−}C_5H_{9-\alpha}(OOH)_\alpha O_2$ with α = 1 (6), (c) Consecutive Steps for $O,O\text{−}C_6H_{9-x}(OOH)_xO_2$ with x = 1 (5), (d) Consecutive Steps for $O\text{−}C_5H_{9-\alpha}(OOH)_\alpha O_2$ with α = 1 (6), and (e) Consecutive Steps for $O,O\text{−}C_6H_{9-x}(OOH)_xO_2$ with x = 2 (10)

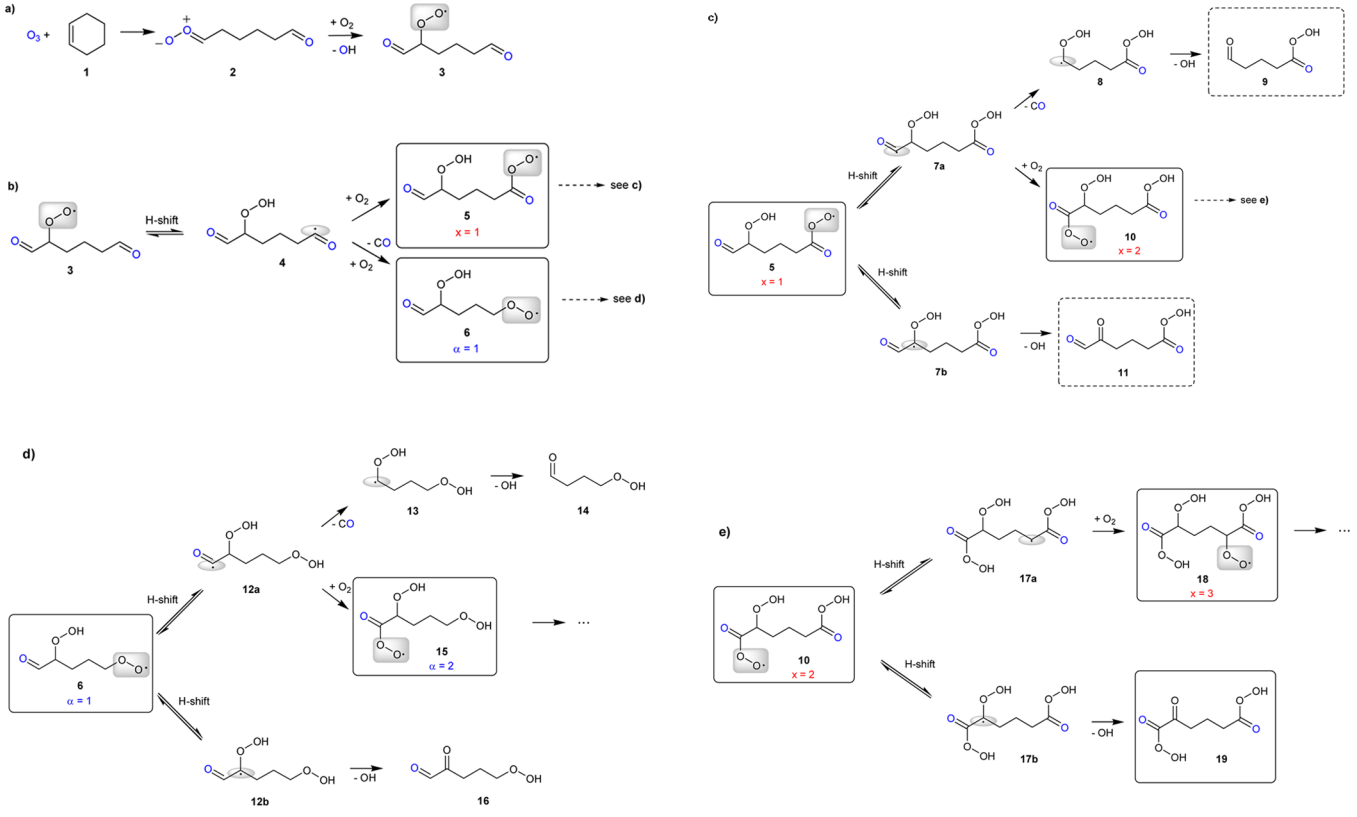

DOI: 10.1021/acs.jpca.5b07295
J. Phys. Chem. A 2015, 119, 10336−10348

Preferred position for the H-abstraction is the aldehydic H atom with the weakest C−H bond.[17,41] The formed acyl radical (**4**) undergoes either direct O_2 addition forming (**5**) or decomposes (CO splitting-off) forming (**6**) after subsequent O_2 addition.[42] The calculated rate coefficient for the acyl radical decomposition, (**4**) → (**6**), is relatively small (k_{298K} = 510 s^{-1}).[13] Assuming $k_{O2} = 10^{-12}$ cm^3 $molecule^{-1}$ s^{-1},[43] $k_{O2} \times [O_2] = 5 \times 10^6$ s^{-1} follows for (**4**) → (**5**) under atmospheric conditions pointing to a predominance of direct O_2 addition for the fate of (**4**). On the other hand, experimental findings of this work (Figure 6) show a substantial fraction of RO_2 radicals formed after CO splitting-off, i.e., $O{-}C_5H_{9-\alpha}(OOH)_\alpha O_2$ with α = 1 (**6**) and α = 2 (**15**). This indicates that the acyl radical decomposition is not negligible in the branching (**4**) → (**5**) vs (**4**) → (**6**).

For the RO_2 radical (**5**) there are two preferred positions for internal H-abstraction,[17,41] namely, the second aldehydic H atom leading to the formation of (**7a**) or the H atom located at the carbon with the OOH group forming (**7b**). The carbonyl radical (**7a**) can again undergo decomposition (CO splitting-off) forming (**8**) in competition with O_2 addition forming (**10**). The rate coefficient for (**7a**) → (**8**) is calculated to be k_{298K} = 3.3 × 10^6 s^{-1},[13] indicating a comparable reaction rate of this step with the O_2 addition (**7a**) → (**10**) with $k_{O2} \times [O_2] = 5 \times 10^6$ s^{-1}. The two species (**7b**) and (**8**) decompose quickly (OH-radical splitting-off) forming the corresponding carbonyl compounds (**9**) and (**11**), respectively.[13,17]

For the further reactions of the RO_2 radical (**6**) (Scheme 1d), the same pathways are assumed as stated for (**5**) in Scheme 1c caused by similar chemical structures in the molecule. Experimental evidence exists only for the occurrence of $O{-}C_5H_{9-\alpha}(OOH)_\alpha O_2$ with α = 2 (**15**). The end products (**14**) and (**16**) are not detectable with the ionization techniques applied here. Evidence for the formation of (**14**) and (**16**) is subject of ongoing research.

The RO_2 radical (**10**) (Scheme 1e) can internally abstract the H atom in β-position to the peroxy carboxylic group forming the RO_2 radical (**18**) after O_2 addition of (**17a**), or it can abstract the H atom located at the carbon with the OOH group forming (**17b**). Reaction (**10**) → (**17a**) represents a 1,7 H-shift, while (**10**) → (**17b**) is a 1,4 H-shift. The latter step is less favorable. Decomposition of (**17b**) yields the closed-shell product $C_6H_8O_7$ (**19**). A product with this composition was detected by means of both ionization techniques; see Figures 3 and S9. It is to be noted that the experiments with variable cyclohexene conversion pointed to a bimolecular step responsible for $C_6H_8O_7$ formation rather than a unimolecular reaction. So, it remains questionable whether (**10**) → (**17b**) → (**19**) contributed significantly to the formation of $C_6H_8O_7$.

This mechanism, Scheme 1a−e, allows to qualitatively describe the formation of the detected highly oxidized RO_2 radicals from the ozonolysis of cyclohexene. For the analogous reactions of cyclopentene, cycloheptene, and cyclooctene, the corresponding RO_2 radicals with a similar behavior were observed. Therefore, this mechanism should be also applicable to these reaction systems. Generally, the formation of all detected RO_2 radicals can be explained by the autoxidation scheme: ROO → QOOH and subsequently QOOH + O_2 → R′OO.[8,10,13,18] The most abundant RO_2 radical with two OOH groups ((**10**) in the cyclohexene system) is most likely formed via successively internal H-abstraction of the aldehydic H atoms ((**3**) → (**4**) and (**5**) → (**7a**) for cyclohexene). Further propagation of the radical chain is hindered by the absence of further, weakly bond H atoms in the cycloalkenes. Hence, only small signals of RO_2 radicals with three OOH groups ((**18**) for cyclohexene) were visible in the mass spectra, see signal E in Figure 2.

3.5. Time Dependence of RO_2 Formation and Total HOM Yields. Time-dependent measurements of RO_2 radical concentrations, $O,O{-}C_6H_{9-x}(OOH)_xO_2$ with x = 1−3, from ozonolysis of cyclohexene in the range 1.5−7.9 s showed that the concentration ratios between these RO_2 radicals are already established after a reaction time of 1.5 s; see an example in Figure 8. This fact points to a fast RO_2 radical interconversion

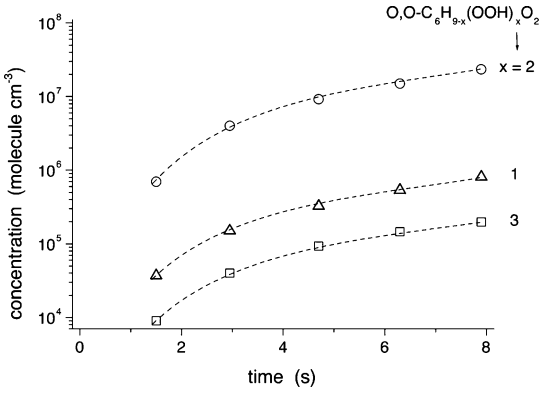

Figure 8. RO_2 radicals from cyclohexene ozonolysis ($O,O{-}C_6H_{9-x}(OOH)_xO_2$ with x = 1−3) as a function of time, nitrate ionization. $[O_3] = 6.1 \times 10^{11}$ and $[c\text{-}C_6H_{10}] = 1.25 \times 10^{12}$ molecules cm^{-3}, reaction time: 1.5−7.9 s.

of (**5**), (**10**), and (**18**). Thus, based on the reaction mechanism shown before, the unimolecular rate coefficients of the intramolecular H-shifts ((**5**) → (**7a**) and (**10**) → (**17a**)) must be larger than 1 s^{-1}. This estimate assumes that the O_2 addition of the corresponding QOOH ((**7a**) → (**10**) and (**17a**) → (**18**)) with a first-order rate coefficient of about 5 × 10^6 s^{-1} at atmospheric O_2 concentration[43] is much faster than the QOOH reverse reaction ((**7a**) → (**5**) and (**17a**) → (**10**)). Calculated rate coefficients from literature[13] for the intramolecular H-shift (**5**) → (**7a**) of 0.5 s^{-1} and for (**10**) → (**17a**) of 0.045 s^{-1} are lower than the ones found in this study.

The time-dependent measurements revealed on the one hand a rapid RO_2 radical interconversion, but on the other hand they showed an interesting behavior of the individual RO_2 concentrations with time. For constant reaction conditions (constant reactant concentrations) the RO_2 radical concentrations increased by a factor of 20−35 when increasing the reaction time from 1.5 to 7.9 s (i.e., by a factor about 5). A nearly proportional increase of RO_2 radical concentrations with time was expected for conditions of negligible RO_2 consuming steps (RO_2 + R′O_2, etc.). The stronger increase with time indicates a rate limited entrance channel for the highly oxidized RO_2 radicals followed by rapid RO_2 radical interconversion. This becomes more clear from measurements of total RO_2 radical concentrations ($O,O{-}C_6H_{9-x}(OOH)_xO_2$ with x = 2 mainly) as a function of reacted cyclohexene for different reaction times. Figure 9 shows the measurements at 1.5, 2.95, 6.3, and 7.9 s for converted cyclohexene <5 × 10^8 molecules cm^{-3} using nitrate ionization. The measured concentrations of closed-shell products and $O{-}C_5H_{9-\alpha}(OOH)_\alpha O_2$ radicals (nitrate ionization) were negligible under these conditions.

DOI: 10.1021/acs.jpca.5b07295
J. Phys. Chem. A 2015, 119, 10336−10348

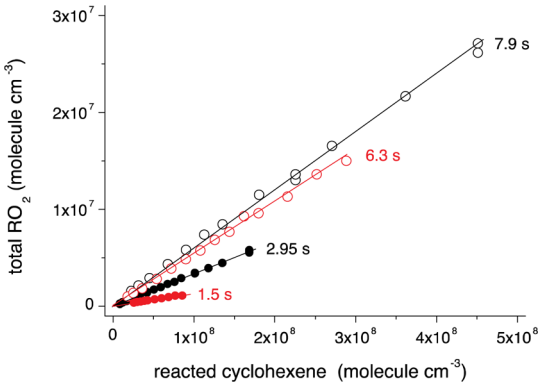

Figure 9. Total RO_2 concentrations $O,O-C_6H_{9-x}(OOH)_xO_2$ (mainly with x = 2) as a function of reacted cyclohexene at different reaction times, nitrate ionization. The straight lines show the results from linear regression analysis used to determine the total RO_2 formation yields. $[O_3] = 6.1 \times 10^{11}$ and $[c\text{-}C_6H_{10}] = (6.3-125) \times 10^{10}$ molecules cm^{-3}.

Resulting molar formation yields of RO_2 radicals from linear regression analysis of the data given in Figure 9 are 1.37 ± 0.04% (1.5 s), 3.35 ± 0.02% (2.95 s), 5.4 ± 0.1% (6.3 s), and 6.0 ± 0.1% (7.9 s). From these results it can be expected that for reaction times longer than about 10 s the rate limited entrance step is fast enough resulting in time-independent RO_2 formation yields. Such a pathway can be describes kinetically with a first-order reaction with a rate coefficient of about 0.3 s^{-1}, i.e., $\exp(-10\ s \times 0.3\ s^{-1}) < 0.05$. The chemical nature of this entrance step is highly speculative at the moment. It should be located between the formation of (**3**) and (**5**).

In Figure 10, the total HOM concentrations (RO_2 radicals and closed-shell species) are depicted as a function of reacted

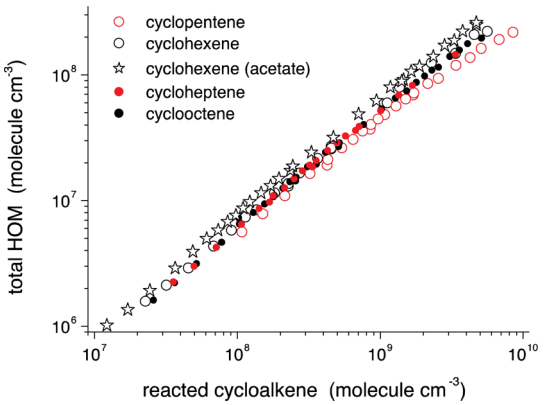

Figure 10. Total HOM concentration as a function of reacted cycloalkene, nitrate ionization (open stars: acetate ionization), reaction time = 7.9 s.

cycloalkene for all measurement series determined at a reaction time of 7.9 s. The total HOM concentrations show a slight curvature with increasing cycloalkene conversion probably due to the fact that not all products from $RO_2 + R'O_2$ reactions (becoming more important for high amounts of reacted cycloalkene) were detected (or detected with lower sensitivity). For reacted cycloalkene $< 5 \times 10^8$ molecules cm^{-3}, linear regression analysis yielded the molar HOM formation yields of 4.8 ± 0.2% (cyclopentene), 6.0 ± 0.1% (cyclohexene), 5.9 ± 0.1% (cycloheptene), and 5.9 ± 0.1% (cyclooctene) using nitrate ionization and 7.3 ± 0.2% (cyclohexene) from acetate ionization. Given error limits represent 2σ values of the statistical error from regression analysis. The yields have to be treated as lower limit values affected with a calibration uncertainty by a factor of 2. Molar HOM formation yields of 4 ± 2%[8] and 4.5 ± 3.8%[13] are reported in the literature from cyclohexene ozonolysis based on analysis of closed-shell products (nitrate ionization).

3.6. Reaction of Highly Oxidized RO_2 Radicals ($O,O-C_6H_{9-x}(OOH)_xO_2$ with $x = 2$) with NO_2, NO, and SO_2. The strong signals of RO_2 radicals with two OOH groups, here $O,O-C_6H_7(OOH)_2O_2$ from cyclohexene ozonolysis, allowed to study their reactions with the atmospherically relevant trace gases NO_2, NO, and SO_2.

NO_2: With increasing NO_2 concentrations in the reaction gas, an increasing signal in the spectrum appeared, which could be attributed to the corresponding peroxynitrate formed via $O,O-C_6H_7(OOH)_2O_2 + NO_2 \rightarrow O,O-C_6H_7(OOH)_2O_2NO_2$.[44] This substance is likely an acyl-type peroxynitrate due to the expected structure of the RO_2 radical (**10**). Thermal lifetimes of acyl peroxynitrates are in the order of 0.5–1 h at 298 K.[45,46] The concentrations of RO_2 radicals and the peroxynitrate as a function of NO_2 are depicted in

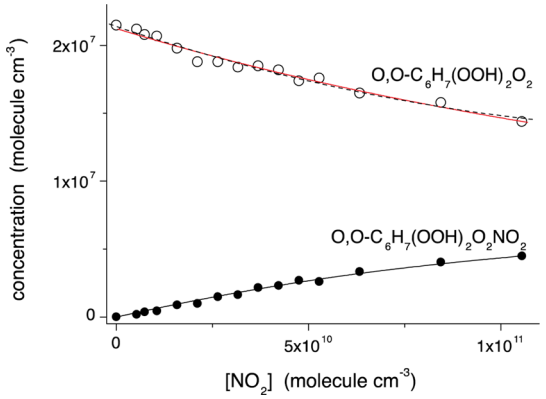

Figure 11. Concentrations of $O,O-C_6H_7(OOH)_2O_2$ and $O,O-C_6H_7(OOH)_2O_2NO_2$ as a function of the NO_2 concentration from ozonolysis of cyclohexene, nitrate ionization. The dashed black line represents the quadratic equation $[RO_2] = a + b[NO_2] + c[NO_2]^2$ and the full black line the result from regression analysis according to eq III with $y(RO_2NO_2) = 0.67 \pm 0.02$. The red curve shows the best-fit result from the determination of k_{NO2}. $[O_3] = 6.1 \times 10^{11}$ and $[c\text{-}C_6H_{10}] = 1.26 \times 10^{12}$ molecules cm^{-3}, reaction time: 7.9 s.

Figure 11. The RO_2NO_2 formation yield was determined with 0.67 ± 0.02 from regression analysis according to eq III,

$$[RO_2NO_2] = y(RO_2NO_2) \times \text{reacted}[RO_2] = y(RO_2NO_2) \times (-b[NO_2] - c[NO_2]^2) \quad \text{(III)}$$

where the measurement points $[RO_2] = f([NO_2])$ are represented by a quadratic equation, $[RO_2] = a + b[NO_2] + c[NO_2]^2$, allowing a more robust calculation of $y(RO_2NO_2)$; $a = 2.14 \times 10^7$ molecules cm^{-3}, $b = -9.49 \times 10^{-5}$, and $c = 2.93 \times 10^{-16}$ cm^3 $molecule^{-1}$.

The RO_2NO_2 yield of 0.67 ± 0.02 describes very well the RO_2NO_2 formation (full black line) in the whole measurement range. This good correlation indicates that the RO_2 formation process for $O,O-C_6H_7(OOH)_2O_2$ (**10**) was not significantly affected by any other NO_2 reactions with precursors of (**10**),

DOI: 10.1021/acs.jpca.5b07295
J. Phys. Chem. A 2015, 119, 10336–10348

$[NO_2] \leq 1.1 \times 10^{11}$ molecules cm^{-3}. (Lowering of O,O−$C_6H_7(OOH)_2O_2$ (**10**) formation by unwanted NO_2 reactions would lead to a seeming decrease of the RO_2NO_2 yield with increasing NO_2 concentrations.)

The fact that the observed RO_2 disappearance with increasing NO_2 was predominantly caused by the RO_2 + NO_2 reaction allowed for a kinetic analysis of the reaction. Measured time-dependent O,O−$C_6H_7(OOH)_2O_2$ concentrations (in absence of NO_2) showed virtually a square dependence on time, $[RO_2] = 0.5 \text{ const} \times t^2$ (see Figure S11), resulting in the term "const × t" describing the RO_2 formation rate in eq IV.

$$\frac{d[RO_2]}{dt} = \text{const} \times t - k_{NO2}[RO_2][NO_2] \quad \text{(IV)}$$

Eq IV was integrated numerically for [0; 7.9 s] by a semi-implicit extrapolation method connected with a Newton technique[47] for determining the free parameters "const" and "k_{NO2}" in a least-squares analysis minimize the difference between measured and calculated $[RO_2] = f([NO_2])$. The best-fit result yielded const = $(6.8 \pm 0.1) \times 10^5$ molecules cm^{-3} s^{-2} and $k_{NO2} = (1.6 \pm 0.1) \times 10^{-12}$ cm^3 $molecule^{-1}$ s^{-1}; see the red line in Fig. 11. Given uncertainties comprise two standard deviations of statistical errors. Additional systematic errors (uncertainties of the reaction time in the free-jet system[19] and the NO_2 concentration) were assumed to be ≤25% in total leading to an extension of the error limit, $k_{NO2} = (1.6 \pm 0.5) \times 10^{-12}$ cm^3 $molecule^{-1}$ s^{-1}. This value of the rate coefficient for the O,O−$C_6H_7(OOH)_2O_2$ + NO_2 reaction is about a factor of 5 smaller than the recommended rate coefficient for $C_2H_5O_2$ + NO_2[43] at T = 298 K, and a factor of 6 smaller than the rate coefficient for $CH_3C(O)O_2$ + NO_2[48] at T = 295 K. For larger RO_2 radicals there are no experimental data available in the literature.

NO: With increasing NO concentration an increasing signal of a new product appeared in the spectrum consistent with the formation of the corresponding organic nitrate, O,O−$C_6H_7(OOH)_2O_2$ + NO → O,O−$C_6H_7(OOH)_2ONO_2$;[49] see Figure 12. The $RONO_2$ formation yield was determined according to eq V approximating again the measurements

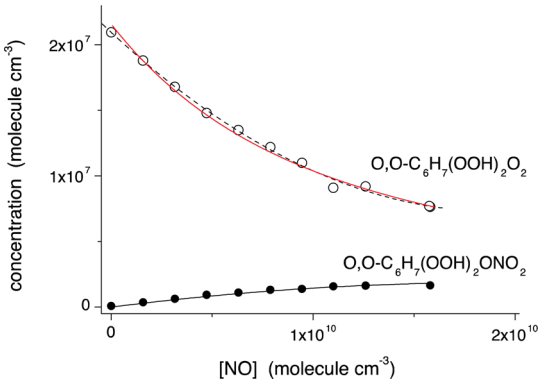

Figure 12. Concentrations of O,O−$C_6H_7(OOH)_2O_2$ and O,O−$C_6H_7(OOH)_2ONO_2$ as a function of the NO concentration from ozonolysis of cyclohexene, nitrate ionization. The dashed black line represents the quadratic equation $[RO_2] = a + b[NO_2] + c[NO_2]^2$ describing the measured $[RO_2] = f([NO])$, the full black line the result from regression analysis according to eq V and the red curve the best-fit result from the determination of k_{NO}. $[O_3] = 8.6 \times 10^{10}$ and [c-C_6H_{10}] = 9.1×10^{12} molecules cm^{-3}, reaction time: 7.9 s.

$[RO_2] = f([NO])$ by a quadratic equation, $a = 2.09 \times 10^7$ molecules cm^{-3}, $b = -1.43 \times 10^{-3}$, $c = 3.73 \times 10^{-14}$ cm^3 $molecule^{-1}$, in the same way as described before for RO_2NO_2.

$$[RONO_2] = y(RONO_2) \times \text{reacted}[RO_2] = y(RONO_2) \times (-b[NO] - c[NO]^2) \quad \text{(V)}$$

The resulting $RONO_2$ yield of 0.14 ± 0.01 is close to reported formation yields of 0.17 ± 0.03 and 0.21 ± 0.03 for corresponding organic nitrates from the reaction of C_6-alkyl peroxy radicals with NO.[49] Kinetic analysis by means of eq VI has been performed analogously to the approach described for the RO_2 + NO_2 reaction.

$$\frac{d[RO_2]}{dt} = \text{const} \times t - k_{NO}[RO_2][NO] \quad \text{(VI)}$$

The best-fit result yielded to const = $(6.9 \pm 0.3) \times 10^5$ molecules cm^{-3} s^{-2} and $k_{NO} = (3.4 \pm 0.2) \times 10^{-11}$ cm^3 $molecule^{-1}$ s^{-1} (2σ error limits). Assuming again additional systematic errors due to uncertainties of the reaction time and the NO concentration of ≤25%, the error limits have to be extended, leading to $k_{NO} = (3.4 \pm 0.9) \times 10^{-11}$ cm^3 $molecule^{-1}$ s^{-1}. This value is somewhat higher than rate coefficients of other RO_2 + NO reactions reported in the literature. For instance, for the reaction $C_2H_5O_2$ + NO a rate coefficient $k = (8.9 \pm 3.0) \times 10^{-12}$ cm^3 $molecule^{-1}$ s^{-1}[43] was measured and for $CH_3C(O)O_2$ + NO a value $k = (2.0 \pm 0.3) \times 10^{-11}$ cm^3 $molecule^{-1}$ s^{-1}.[48]

SO_2: SO_2 additions of up to 10^{13} molecules cm^{-3} did not cause any measurable effect on the RO_2 radical concentration, see Figure 13. There were also no indications for the formation

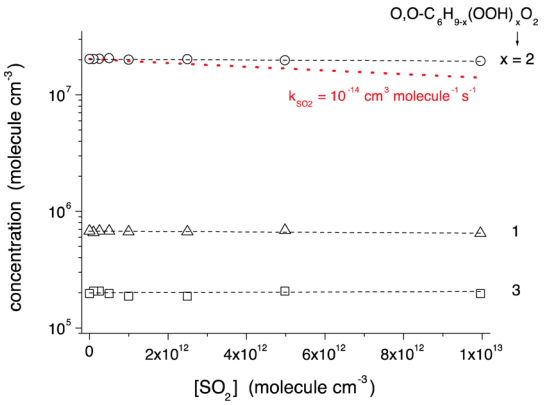

Figure 13. Concentrations of O,O−$C_6H_{9-x}(OOH)_xO_2$ radicals for x = 1−3 as a function of the SO_2 concentration from ozonolysis of cyclohexene, nitrate ionization. The red dotted line shows the result of calculations assuming $k_{SO2} = 10^{-14}$ cm^3 $molecule^{-1}$ s^{-1}. $[O_3] = 6.1 \times 10^{11}$ and [c-C_6H_{10}] = 1.26×10^{12} molecules cm^{-3}, reaction time: 7.9 s.

of new products in the mass spectra. Thus, the reactivity of the highly oxidized RO_2 radicals toward SO_2 is quite small. A rough estimate suggests that the corresponding rate coefficient for RO_2 + SO_2 must be $<10^{-14}$ cm^3 $molecule^{-1}$ s^{-1}. The dotted red line in Figure 13 shows the expected RO_2 radical decay assuming $k_{SO2} = 10^{-14}$ cm^3 $molecule^{-1}$ s^{-1}. The calculation has been done solving the corresponding differential equation for the RO_2 + SO_2 reaction (analogous to eqs IV and VI) for a given k_{SO2}; const = $2[RO_2]/t^2$ at $[SO_2] = 0$. A rate coefficient $<10^{-14}$ cm^3 $molecule^{-1}$ s^{-1} for the reaction of O,O−$C_6H_7(OOH)_2O_2$ with SO_2 is in line with the reactivity of

DOI: 10.1021/acs.jpca.5b07295
J. Phys. Chem. A 2015, 119, 10336−10348

other RO_2 radicals toward SO_2. Sander and Watson[50] reported an upper limit of 5×10^{-17} cm^3 molecule^{-1} s^{-1} for the reaction $CH_3O_2 + SO_2$. Theoretical calculations do support very low rate coefficients for $RO_2 + SO_2$ caused by energy barriers of ~10 kcal mol^{-1} or higher.[51]

The kinetic measurements of the reaction of O,O–$C_6H_7(OOH)_2O_2$ with NO_2, NO and SO_2 revealed a RO_2 reactivity of this highly oxidized species similar to the known reactivity of relatively small "simple" RO_2 radicals in the literature. The rate coefficient of the NO_2 reaction from this study is smaller by a factor of 5–6 regarding literature values of other RO_2 radicals,[43,48] while the rate coefficient of the reaction with NO was measured to be somewhat higher. Thus, also these highly oxidized RO_2 radicals do effectively react with NO contributing to organic nitrate formation in the atmosphere. The $RONO_2$ yields from highly oxidized RO_2 radicals, 0.14 ± 0.01 from the selected C_6-species of this study and 0.27–0.32 from C_{10}-species from our former study,[10] are in line with the trend of increasing $RONO_2$ yields with larger C-skeletons of the molecule.[49] Measurements in the presence of SO_2 confirm that the reaction of highly oxidized RO_2 radicals with SO_2 is negligible for SO_3 production and subsequently for H_2SO_4 formation in the atmosphere.

4. CONCLUSIONS

The reaction of ozone with C_5–C_8 cycloalkenes in air forms highly oxidized RO_2 radicals with the general formula O,O–$C_nH_{2n-3-x}(OOH)_xO_2$ with n = 5–8 (number of the carbon atoms) and x = 1–3 (number of OOH groups in the molecule). "O,O" stands for two O atoms arising from the attacking ozone. The most abundant RO_2 radicals detected contain two OOH groups, most likely from intramolecular H-shifts of aldehydic H atoms. Their formation proceeds on a time scale of seconds for atmospheric reactant conditions. The formation mechanism of all detected RO_2 radicals can be explained by an autoxidation scheme: ROO → QOOH and subsequent reaction of QOOH with O_2 forming the next peroxy radical, QOOH + O_2 → R′OO. From experiments with O,O–$C_6H_7(OOH)_2O_2$ it can be concluded that these RO_2 radicals have nearly the same reactivity toward NO_2, NO, and SO_2 as known in the literature for "simple" RO_2 radicals.

■ ASSOCIATED CONTENT

Supporting Information

The Supporting Information is available free of charge on the ACS Publications website at DOI: 10.1021/acs.jpca.5b07295.

Figure S1a: Nitrate charger ion spectrum; Figure S1b: Acetate charger ion spectrum; Figure S1c: Acetate, $^{13}CH_3COO^-$, charger ion spectrum; Figure S2: Mass spectra recorded in absence or presence of D_2O; Figure S3: Accretion products from cyclohexene ozonolysis; Figure S4a: RO_2 radicals and closed-shell products from cyclopentene ozonolysis; Figure S4b: Accretion products from cyclopentene ozonolysis; Figure S5a: RO_2 radicals and closed-shell products from cycloheptene ozonolysis; Figure S5b: Accretion products from cycloheptene ozonolysis; Figure S6a: RO_2 radicals and closed-shell products from cyclooctene ozonolysis; Figure S6b: Accretion products from cyclooctene ozonolysis; Figures S7 and S8: Results from peak fitting; Figure S9: Comparison of concentrations of closed-shell molecules and accretion products from cyclohexene ozonolysis obtained by acetate or nitrate ionization; Figure S10: Concentrations of $C_5H_8O_4$ and $C_6H_8O_5$ as a function of reacted cyclohexene (acetate ionization); Figure S11: O,O–$C_6H_7(OOH)_2O_2$ concentrations from cyclohexene ozonolysis as a function of time (PDF)

■ AUTHOR INFORMATION

Corresponding Author

*E-mail: berndt@tropos.de.

Notes

The authors declare no competing financial interest.

■ ACKNOWLEDGMENTS

The authors thank K. Pielok and A. Rohmer for technical assistance as well as M. Ehn for fruitful discussions.

■ REFERENCES

(1) Calvert, J. G.; Atkinson, R.; Kerr, J. A.; Madronich, S.; Moortgat, G. K.; Wallington, T. J.; Yarwood, G. *The Mechanisms of Atmospheric Oxidation of the Alkenes*; Oxford University Press: Oxford, 2000.

(2) Guenther, A.; Hewitt, C. N.; Erickson, D.; Fall, R.; Geron, C.; Graedel, T.; Harley, P.; Klinger, L.; Lerdau, M.; McKay.; et al. A Global Model of Natural Volatile Organic Compound Emissions. *J. Geophys. Res.* **1995**, *100*, 8873–8892.

(3) Hofzumahaus, A.; Rohrer, F.; Lu, K.; Bohn, B.; Brauers, T.; Chang, C.; Fuchs, H.; Holland, F.; Kita, K.; Kondo, Y.; et al. Amplified Trace Gas Removal in the Troposphere. *Science* **2009**, *324*, 1702–1704.

(4) Riipinen, I.; Yli-Juuti, T.; Pierce, J. R.; Petäjä, T.; Worsnop, D. R.; Kulmala, M.; Donahue, N. M. The Contribution of Organics to Atmospheric Nanoparticle Growth. *Nat. Geosci.* **2012**, *5*, 453–458.

(5) Eisele, F. L.; Tanner, D. J. Ion-assisted Tropospheric OH Measurements. *J. Geophys. Res.* **1991**, *96*, 9295–9308.

(6) Jokinen, T.; Sipilä, M.; Junninen, H.; Ehn, M.; Lönn, G.; Hakala, J.; Petäjä, T.; Mauldin, R. L., III; Kulmala, M.; Worsnop, D. R. Atmospheric Sulphuric acid and Neutral Cluster Measurements using CI-APi-TOF. *Atmos. Chem. Phys.* **2012**, *12*, 4117–4125.

(7) Ehn, M.; Kleist, E.; Junninen, H.; Petäjä, T.; Lönn, G.; Schobesberger, S.; Dal Maso, M.; Trimborn, A.; Kulmala, M.; Worsnop, D. R.; et al. Gas Phase Formation of Extremely Oxidized Pinene Reaction Products in a Chamber and Ambient Air. *Atmos. Chem. Phys.* **2012**, *12*, 5113–5127.

(8) Ehn, M.; Thornton, J. A.; Kleist, E.; Sipilä, M.; Junninen, H.; Pullinen, I.; Springer, M.; Rubach, F.; Tillmann, R.; Lee, B.; et al. A Large Source of Low-Volatility Secondary Organic Aerosol. *Nature* **2014**, *506*, 476–479.

(9) Donahue, N. M.; Kroll, J. H.; Pandis, S. N.; Robinson, A. L. A Two-Dimensional Volatility Basis Set – Part 2: Diagnostics of Organic-Aerosol Evolution. *Atmos. Chem. Phys.* **2012**, *12*, 615–634.

(10) Jokinen, T.; Sipilä, M.; Richters, S.; Kerminen, V.-M.; Paasonen, P.; Stratmann, F.; Worsnop, D. R.; Kulmala, M.; Ehn, M.; Herrmann, H.; et al. Rapid Autoxidation Forms Highly Oxidized RO_2 Radicals in the Atmosphere. *Angew. Chem., Int. Ed.* **2014**, *53*, 14596–14600.

(11) Jazukowitsch, H. N. 226. Mitteilung: A. Kuhlberg aus St. Petersburg. Sitzung der Russischen Chemischen Gesellschaft vom 1./13. Mai 1875. *Ber. Dtsch. Chem. Ges.* **1875**, *8*, 766–769.

(12) Staudinger, H. Über die Autoxydation Organischer Verbindungen, III.: Über Autoxydation des Asymm. Diphenyl-Äthylens. *Ber. Dtsch. Chem. Ges. B* **1925**, *58*, 1075–1079.

(13) Rissanen, M. P.; Kurten, T.; Sipilä, M.; Thornton, J. A.; Kangasluoma, J.; Sarnela, N.; Junninen, H.; Jorgensen, S.; Schallhart, S.; Kajos, M. K.; et al. The Formation of Highly Oxidized Multifunctional Products in the Ozonolysis of Cyclohexene. *J. Am. Chem. Soc.* **2014**, *136*, 15596–15606.

(14) Pilling, M. J. Interactions Between Theory and Experiment in the Investigation of Elementary Reactions of Importance in Combustion. *Chem. Soc. Rev.* **2008**, *37*, 676–685.

DOI: 10.1021/acs.jpca.5b07295
J. Phys. Chem. A 2015, 119, 10336–10348

(15) Scheer, A. M.; Welz, O.; Zador, J.; Osborn, D. L.; Taatjes, C. A. Low-temperature Combustion Chemistry of Novel Biofuels: Resonance-Stabilized QOOH in the Oxidation of Diethyl Ketone. *Phys. Chem. Chem. Phys.* **2014**, *16*, 13027−13040.
(16) Crounse, J. D.; Knap, H. C.; Ornso, K. B.; Jorgensen, S.; Paulot, F.; Kjaergaard, H. G.; Wennberg, P. O. Atmospheric Fate of Methacrolein. 1. Peroxy Radical Isomerization Following Addition of OH and O_2. *J. Phys. Chem. A* **2012**, *116*, 5756−5762.
(17) Crounse, J. D.; Nielsen, L. B.; Jorgensen, S.; Kjaergaard, H. G.; Wennberg, P. O. Autoxidation of Organic Compounds in the Atmosphere. *J. Phys. Chem. Lett.* **2013**, *4*, 3513−3520.
(18) Mentel, T. F.; Springer, M.; Ehn, M.; Kleist, E.; Pullinen, I.; Kurtén, T.; Rissanen, M. P.; Wahner, A.; Wildt, J. Formation of Highly Oxidized Multifunctional Compounds: Autoxidation of Peroxy Radicals Formed in the Ozonolysis of Alkenes − Deduced from Structure−Product Relationships. *Atmos. Chem. Phys. Discuss.* **2015**, *15*, 2791−2851.
(19) Berndt, T.; Kaethner, R.; Voigtländer, J.; Stratmann, F.; Pfeifle, M.; Reichle, P.; Sipilä, M.; Kulmala, M.; Olzmann, M. Kinetics of the Unimolecular Reaction of CH_2OO and the Bimolecular Reactions with the Water Monomer, Acetaldehyde and Acetone at Atmospheric Conditions. *Phys. Chem. Chem. Phys.* **2015**, *17*, 19862−19873.
(20) Kümmel, W. *Technische Strömungsmechanik − Theorie und Praxis*, 3rd ed.; B.G. Teubner Verlag/GWV Fachverlage GmbH: Wiesbaden, 2007.
(21) Lindinger, W.; Hansel, A.; Jordan, A. Proton-Transfer-Reaction Mass Spectrometry (PTR−MS): Online Monitoring of Volatile Organic Compounds at pptv Levels. *Chem. Soc. Rev.* **1998**, *27*, 347−375.
(22) Greene, C. R.; Atkinson, R. Rate Constants for the Gas-Phase Reactions of O_3 with a Series of Alkenes at 296 ± 2 K. *Int. J. Chem. Kinet.* **1992**, *24*, 803−811.
(23) Treacy, J.; Curley, M.; Wenger, J.; Sidebottom, H. Determination of Arrhenius Parameters for the Reactions of Ozone with Cycloalkenes. *J. Chem. Soc., Faraday Trans.* **1997**, *93*, 2877−2881.
(24) Eisele, F.; Tanner, D. Measurement of the Gas Phase Concentration of H_2SO_4 and Methane Sulfonic Acid and Estimates of H_2SO_4 Production and Loss in the Atmosphere. *J. Geophys. Res.* **1993**, *98*, 9001−9010.
(25) Junninen, H.; Ehn, M.; Petäjä, T.; Luosujärvi, L.; Kotiaho, T.; Kostiainen, R.; Rohner, U.; Gonin, M.; Fuhrer, K.; Kulmala, M.; et al. A High-Resolution Mass Spectrometer to Measure Atmospheric Ion Composition. *Atmos. Meas. Tech.* **2010**, *3*, 1039−1053.
(26) Hyttinen, N.; Kupiainen-Määttä, O.; Rissanen, M. P.; Muuronen, M.; Ehn, M.; Kurtén, T. Modeling the Detection of Highly Oxidized Cyclohexene Ozonolysis Products Using Nitrate-based Chemical Ionization. *J. Phys. Chem. A* **2015**, *119*, 6339−6345.
(27) Berndt, T.; Jokinen, T.; Sipilä, M.; Mauldin, R. L., III; Herrmann, H.; Stratmann, F.; Junninen, H.; Kulmala, M. H_2SO_4 Formation from the Gas-phase Reaction of Stabilized Criegee Intermediates with SO_2: Influence of Water Vapour Content and Temperature. *Atmos. Environ.* **2014**, *89*, 603−612.
(28) Berresheim, H.; Elste, T.; Plass-Dülmer, C.; Eisele, F. L.; Tanner, D. J. Chemical Ionization Mass Spectrometer for Long-Term Measurements of Atmospheric OH and H_2SO_4. *Int. J. Mass Spectrom.* **2000**, *202*, 91−109.
(29) Viggiano, A. A.; Seeley, J. V.; Mundis, P. L.; Williamson, J. S.; Morris, A. M. Rate Constants for the Reactions of $XO_3^-(H_2O)_n$ (X = C, HC, and N) and $NO_3^-(HNO_3)_n$ with H_2SO_4: Implications for Atmospheric Detection of H_2SO_4. *J. Phys. Chem. A* **1997**, *101*, 8275−8278.
(30) Veres, P.; Roberts, J. M.; Warneke, C.; Welsh-Bon, D.; Zahniser, M.; Herndon, S.; Fall, R.; de Gouw, J. Development of Negative-Ion Proton-Transfer Chemical-Ionization Mass Spectrometry (NI-PT-CIMS) for the Measurement of Gas-Phase Organic Acids in the Atmosphere. *Int. J. Mass Spectrom.* **2008**, *274*, 48−55.
(31) Bertram, T. H.; Kimmel, J. R.; Crisp, T. A.; Ryder, O. S.; Yatavelli, R. L. N.; Thornton, J. A.; Cubison, M. J.; Gonin, M.; Worsnop, D. R. A Field-Deployable, Chemical Ionization Time-Of-Flight Mass Spectrometer. *Atmos. Meas. Tech.* **2011**, *4*, 1471−1479.
(32) Lopez-Hilfiker, F. D.; Mohr, C.; Ehn, M.; Rubach, F.; Kleist, E.; Wildt, J.; Mentel, Th. F.; Carrasquillo, A.; Daumit, K.; Hunter, J.; et al. Phase Partitioning and Volatility of Secondary Organic Aerosol Components Formed from α-Pinene Ozonolysis and OH Oxidation: The Importance of Accretion Products and other Low Volatility Compounds. *Atmos. Chem. Phys. Discuss.* **2015**, *15*, 4463−4494.
(33) Graul, S. T.; Schnute, M. E.; Squires, R. R. Gas-Phase Acidities of Carboxylic-Acids and Alcohols from Collision-Induced Dissociation of Dimer Cluster Ions. *Int. J. Mass Spectrom. Ion Processes* **1990**, *96*, 181−198.
(34) Atkinson, R.; Aschmann, S. M. OH Production from the Gas-Phase Reactions of O_3 with a Series of Alkenes under Atmospheric Conditions. *Environ. Sci. Technol.* **1993**, *27*, 1357−1363.
(35) Yu, J.; Jeffries, H. E.; Sexton, K. G. Atmospheric Photooxidation of Alkylbenzenes − 1. Carbonyl Product Analysis. *Atmos. Environ.* **1997**, *31*, 2261−2280.
(36) Huang, M.; Hu, X.; Guo, X.; Gu, X.; Zhao, W.; Wang, Z.; Fang, L.; Zhang, W. Chemical Composition of Gas and Particle−Phase Products of OH−Initiated Oxidation of 1,3,5-Trimethylbenzene. *Atmos. Pollut. Res.* **2014**, *5*, 73−78.
(37) Jokinen, T.; Berndt, T.; Makkonen, R.; Kerminen, V.-M.; Junninen, H.; Paasonen, P.; Stratmann, F.; Herrmann, H.; Guenther, A.; Worsnop, D. R.; et al. Production of Extremely Low-Volatile Organic Compounds from Biogenic Emissions: Measured Yields and Atmospheric Implications. *Proc. Natl. Acad. Sci. U. S. A.* **2015**, *112*, 7123−7128.
(38) Criegee, R. Mechanism of Ozonolysis. *Angew. Chem., Int. Ed. Engl.* **1975**, *14*, 745−752.
(39) Donahue, N. M.; Kroll, J. H.; Anderson, J. G.; Demerjian, K. L. Direct Observation of OH Production from the Ozonolysis of Olefins. *Geophys. Res. Lett.* **1998**, *25*, 59−62.
(40) Kroll, J. H.; Sahay, S. R.; Anderson, J. G.; Demerjian, K. L.; Donahue, N. M. Mechanism of HO_x Formation in the Gas-Phase Ozone-Alkene Reaction. 2. Prompt versus Thermal Dissociation of Carbonyl Oxides to Form OH. *J. Phys. Chem. A* **2001**, *105*, 4446−4457.
(41) Benson, S. W. *Thermochemical Kinetics*, 2nd ed.; Wiley Interscience: New York, 1976.
(42) Cadman, P.; Dodwell, C.; Trotman-Dickenson, A. F.; White, A. J. The Kinetics of Hydrogen Abstraction by Difluoroamino-Radicals, from Propionaldehyde, and n- and iso-Butyraldehyde, and their Acyl Radical Decompositions. *J. Chem. Soc. A* **1970**, 2371−2376.
(43) Lightfoot, P. D.; Cox, R. A.; Crowley, M.; Hayman, G. D.; Zabel, F. Organic Peroxy Radicals: Kinetics, Spectroscopy and Tropospheric Chemistry. *Atmos. Environ., Part A* **1992**, *26*, 1805−1961.
(44) Zabel, F.; Reimer, A.; Becker, K.-H.; Fink, E. H. Thermal Decomposition of Alkyl Peroxynitrates. *J. Phys. Chem.* **1989**, *93*, 5500−5507.
(45) Kirchner, K.; Mayer-Figge, A.; Zabel, F.; Becker, K.-H. Thermal Stability of Peroxynitrates. *Int. J. Chem. Kinet.* **1999**, *31*, 127−144.
(46) Kabir, M.; Jagiella, S.; Zabel, F. Thermal Stability of n-Acyl Peroxynitrates. *Int. J. Chem. Kinet.* **2014**, *46*, 462−469.
(47) Stoer, J.; Bulirsch, R. *Einführung in die Numerische Mathematik II*; Springer Verlag: Berlin, 1978.
(48) Sehested, J.; Christensen, L. K.; Mogelberg, T.; Nielsen, O. J.; Wallington, T. J.; Guschin, A.; Orlando, J. J.; Tyndall, G. S. Absolute and Relative Rate Constants for the Reactions $CH_3C(O)O_2$ + NO and $CH_3C(O)O_2$ + NO_2 and Thermal Stability of $CH_3C(O)O_2NO_2$. *J. Phys. Chem. A* **1998**, *102*, 1779−1789.
(49) Atkinson, R.; Aschmann, S. M.; Carter, W. L. P.; Winer, A. M.; Pitts, J. N. Alkyl Nitrate Formation from the NO_x-Air Photooxidations of C_2-C_8 n-Alkanes. *J. Phys. Chem.* **1982**, *86*, 4563−4569.
(50) Sander, S. P.; Watson, R. T. A Kinetic Study of the Reaction of SO_2 with CH_3O_2. *Chem. Phys. Lett.* **1981**, *77*, 473−475.

DOI: 10.1021/acs.jpca.5b07295
J. Phys. Chem. A 2015, 119, 10336−10348

(51) Kurten, T.; Lane, J. R.; Jorgensen, S.; Kjaergaard, H. G. A Computational Study of the Oxidation of SO_2 to SO_3 by Gas-Phase Organic Oxidants. *J. Phys. Chem. A* **2011**, *115*, 8669−8681.

DOI: 10.1021/acs.jpca.5b07295
J. Phys. Chem. A 2015, 119, 10336−10348